

Pairing Fluctuations Determine Low Energy Electronic Spectra in Cuprate Superconductors

Sumilan Banerjee*, T. V. Ramakrishnan*⁺, and Chandan Dasgupta*

* *Department of Physics, Indian Institute of Science, Bangalore 560012, India*

⁺ *Department of Physics, Banaras Hindu University, Varanasi 221005, India*

We describe here a minimal theory of tight binding electrons moving on the square planar Cu lattice of the hole-doped cuprates and mixed quantum mechanically with pairs of them (Cooper pairs). Superconductivity occurring at the transition temperature T_c is the long-range, d -wave symmetry phase coherence of these Cooper pairs. Fluctuations necessarily associated with incipient long-range superconducting order have a generic large-distance behaviour near T_c . We calculate the spectral density of electrons coupled to such Cooper pair fluctuations and show that features observed in Angle Resolved Photo Emission Spectroscopy (ARPES) experiments on different cuprates above T_c as a function of doping and temperature emerge naturally in this description. These include ‘Fermi arcs’ with temperature-dependent length and an antinodal pseudogap which fills up linearly as the temperature increases towards the pseudogap temperature. Our results agree quantitatively with experiment. Below T_c , the effects of nonzero superfluid density and thermal fluctuations are calculated and compared successfully with some recent ARPES experiments, especially the observed *bending* or deviation of the superconducting gap from the canonical d -wave form.

I. INTRODUCTION

High-temperature superconductivity in hole-doped cuprates, accompanied by a ‘pseudogap phase’ as well as other strange phenomena, continues to be an outstanding problem in condensed matter physics for a quarter of a century now [1–3]. Over the years ARPES [4, 5] has uncovered a number of unusual spectral properties of electrons near the Fermi energy with definite in-plane momenta. This low-energy electronic excitation spectrum is of paramount importance for explaining the rich and poorly understood collection of experimental findings [1–3] from thermodynamic, transport and spectroscopic measurements on cuprate superconductors. We show here that the spectral function of electrons with momentum ranging over the *putative* Fermi surface (recovered at high temperatures above the pseudogap temperature scale [6–8]) is strongly affected by their coupling to Cooper pairs. On approaching T_c i.e. the temperature at which the Cooper pair phase stiffness becomes nonzero, the inevitable coupling of electrons with long wavelength (d -wave symmetry) phase fluctuations leads to the observed characteristic low-energy behavior observed in ARPES experiments. The idea that Cooper pair phase fluctuations are important in cuprate superconductivity has a long history; we mention only a few examples. The experimental realization that Cooper pair phase fluctuations are significant for a large regime of hole doping (below optimum doping) and temperature owes largely to the observation of large Nernst effect [9] and enhanced fluctuation diamagnetism [10] by Ong and coworkers. The same physics is implied in the early theoretical work [11] of Emery and Kivelson.

The cuprates [2] (e.g. $\text{La}_{2-x}\text{Sr}_x\text{CuO}_4$) exhibit superconductivity at unusually high temperatures on doping the parent compound, a Mott insulator, with holes (x per Cu site in the above case; Fig.1a shows the square

Cu lattice with lattice spacing a). There is long-standing evidence from the $(\cos k_x a - \cos k_y a)$ dependence of the superconducting gap $\Delta_{\mathbf{k}}$ on the in-plane momentum \mathbf{k} of the low energy electronic excitations (observed, for example, in ARPES experiments [4, 5]) that the pairing involves nearest neighbours on a tight binding lattice. We therefore assume that the basic Cooper pair in hole-doped cuprates is the nearest-neighbour spin singlet. Superconductivity is the long-range phase coherence of these Cooper pairs. The low energy degrees of freedom then are (the electrons and) the complex singlet pair amplitudes

$$\psi_{ij} \equiv \frac{\langle b_{ij} \rangle}{\sqrt{2}} = \frac{1}{2} \langle a_{i\downarrow} a_{j\uparrow} - a_{i\uparrow} a_{j\downarrow} \rangle \equiv \psi_m. \quad (1)$$

Here $a_{i\sigma}$ ($a_{i\sigma}^\dagger$) destroys (creates) an electron with spin σ at the lattice site i , sites i and j are nearest neighbours and the bond between them is uniquely labelled by the bond-centre site m (see Fig.1a). An interaction of the form $C \text{Re}(\psi_m \psi_n^*)$ between nearest-neighbour bonds centered at m and n , with positive C , leads to the observed d -wave symmetry superconductivity [12] below T_c . The crossover temperature $T^*(x)$ below which the equilibrium value $\langle |\psi_m| \rangle$ of the local pair amplitude becomes *significant* is taken to be the ‘pseudogap’ temperature. There is considerable experimental evidence for this view [6–8], though there is also the alternative view that $T^*(x)$ is associated with a new long-range order, e.g. d -density wave [13], time reversal symmetry breaking circulating currents [14], electron nematic order [15], stripes [16] etc.

We work out here the effects of the quantum mechanical coupling between (fermionic) electrons and (bosonic) Cooper pairs of the same electrons. On approaching T_c from above, collective d -wave symmetry superconducting correlations develop among the pairs with a characteristic superconducting coherence length scale ξ which diverges at the second-order transition temperature T_c .

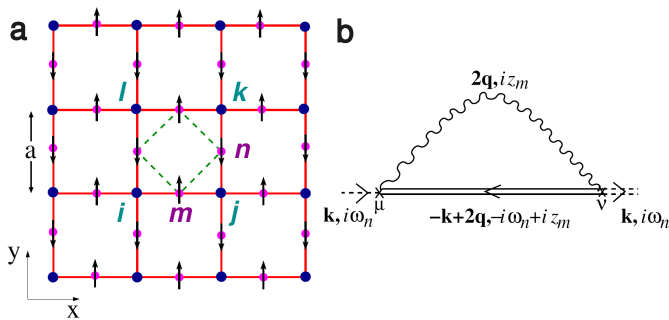


FIG. 1: Square lattice where cuprate superconductivity primarily resides and the pair fluctuation exchange process for the self energy of electrons hopping on it. **a**, The blue circles at $\{\mathbf{R}_i\}$ represent the Cu atoms and the magenta ones at $\{\mathbf{R}_m\}$ (where $\mathbf{R}_m \equiv \mathbf{R}_{ij} \equiv \mathbf{R}_{i\mu}$ with $\hat{\mu} = \hat{x}, \hat{y}$) represent bond centres (also the location of oxygen atoms). The arrows denote planar spins equivalent to $\psi_{ij} = \psi_{i\mu} \equiv \psi_m = \Delta_m \exp(i\theta_m)$ with Δ_m being the length of the ‘spin’ and θ_m the angle it makes with the x -axis; d -wave superconductivity translates in spin language to Ne’el order as shown. **b**, Feynman diagram[26, 27] of the process in which an electron ($\mathbf{k}, i\omega_n$) virtually becomes another electron ($-\mathbf{k} + 2\mathbf{q}, -i\omega_n + iz_m$) and absorbs a Cooper pair ($2\mathbf{q}, iz_m$) in the intermediate state. The curly line denotes the Cooper pair propagator $D_{\mu\nu}(2\mathbf{q}, iz_m)$ (here $z_m = 2m\pi/\beta$ is the bosonic Matsubara frequency, m being an integer).

These correlations have a generic form at large distances (\gg the lattice spacing a). As we show here, the effect of these correlations on the electrons leads, for example, to temperature-dependent Fermi arcs [17] and to the filling of the antinodal pseudogap in the manner observed [18]. Further, the observed long-range order (LRO) below T_c leads to a sharp antinodal spectral feature [19, 20] related to the nonzero superfluid density, and thermal pair fluctuations cause a deviation (‘bending’) of the inferred ‘gap’ as a function of \mathbf{k} from the expected d -wave form ($\cos k_x a - \cos k_y a$). The bending, being of thermal origin, decreases with decreasing temperature, in agreement with some ARPES measurements [21, 22].

We describe the model used for our calculation in Section II, followed by a section (Section III) on the method of calculation and phenomenological inputs that are extracted from various experiments. We have compared our results with a large number ARPES experiments, as mentioned in the preceding paragraph. These are reported in Section IV. There have been many previous studies of the effects of phase fluctuations on electrons; we mention a few of them in the discussion section (Section V) along with some concluding remarks. Our attempt here is based on a particular view of the superconducting transition, does *not* assume preformed d -wave pairs, and a detailed comparison with a large number of ARPES experiments is made. The present paper, in our view, represents a significant development, an extension

of the approach of Ref.[12] to explicitly include electronic (fermion) degrees of freedom in addition to the Cooper pair (bosonic) ones. It also shows that a simple minimal theory can account for a variety of ARPES data, which have hitherto been analyzed separately, using phenomenological [23] or problem specific [24, 25] models. Appendices describe some technical details of our calculations.

II. MODEL

A complete model for electrons in the square planar Cu lattice with relatively weak interlayer coupling and with interactions which strongly affect their motion is needed for describing low energy cuprate phenomena comprehensively. There is no such unanimously accepted description yet. We use a partial, phenomenological model as follows. The electrons are described by the Hamiltonian,

$$\hat{\mathcal{H}} = - \sum_{i,j,\sigma} \tilde{t}_{ij} a_{i\sigma}^\dagger a_{j\sigma} - \sum_{\langle ij \rangle} \tilde{J}_{ij} b_{ij}^\dagger b_{ij}, \quad (2)$$

which consists of a quantum mechanical intersite hopping term, where \tilde{t}_{ij} is the effective amplitude for an electron to hop from site i to site j , and a nearest neighbor pair attraction term with strength \tilde{J}_{ij} . The parameters (i.e. \tilde{t}_{ij} and \tilde{J}_{ij}) of both are strongly affected by correlations.

In the case of strong local repulsion such as large Mott-Hubbard U ($\gg t$) [28], one uses the same form as in its absence, but with renormalized Hamiltonian parameters which are assumed to describe the entire effect of U (at least at low energies). This implies (for example with renormalized hopping \tilde{t}_{ij} replacing t_{ij}) that there are good mobile quasiparticles, albeit with renormalized dispersion. The well known single-site Gutzwiller renormalization factor [28–30], for example, projects out doubly occupied sites completely and is a good approximation for $U \rightarrow \infty$. It assumes, for small hole density x , a multiplicative factor $g_t = 2x/(1+x)$ for t_{ij} and $g_s = 4/(1+x)^2$ for J_{ij} (i.e. $\tilde{t}_{ij} = g_t t_{ij}$ and $\tilde{J}_{ij} = g_s J_{ij}$). The bare hopping amplitude t_{ij} involves the nearest neighbor (t), next-nearest neighbor (t') and further neighbor (t'') hopping terms. In our calculations, we use the above mentioned homogeneous Gutzwiller approximation with standard values for t_{ij} ($t = 300$ meV, $t'/t = -1/4$ and $t'' = 0$, see e.g. [31]). The value of J_{ij} does not appear explicitly in the calculation, as we elucidate later. The J_{ij} term is the well known superexchange (e.g. $J_{ij} \propto t_{ij}^2/U$ in single site Hubbard model [28]) for large U . We have written the conventional $J_{ij} \mathbf{S}_i \cdot \mathbf{S}_j$ term as a pair attraction $-J_{ij} b_{ij}^\dagger b_{ij}$ [32, 33] using the identity $(\mathbf{S}_i \cdot \mathbf{S}_j - \hat{n}_i \hat{n}_j / 4) = -b_{ij}^\dagger b_{ij}$ valid for spin- $\frac{1}{2}$ particles (\mathbf{S}_i and \hat{n}_i are the spin and number operators at site i , respectively). There is thus strong attractive nearest-neighbor spin singlet pairing term in the Hamiltonian, given that the antiferromagnetic coupling J_{ij} is known to be large (~ 1500 K) [34] for undoped cuprates ($x = 0$).

The above identity between nearest-neighbor AF Heisenberg spin interaction and spin singlet Cooper pair attraction means that exact solution of Eq.(2) with either term would lead to the same result. Because of the fact that antiferromagnetic LRO disappears for surprisingly small hole doping x and is replaced by superconducting order, and that the holes are quite mobile, we use the singlet bond pair form in Eq.(2) as being natural and accurate for good approximations, e.g. mean field theory, and assume a homogeneous system as will naturally arise for mobile holes.

Very generally, the bond-pair self interaction term in Eq.(2) can be written via the exact Hubbard-Stratonovich transformation [35] as a time (and space) dependent bond pair potential acting on electrons and characterized by a field $\psi_m(\tau)$ with a Gaussian probability distribution [here τ is the imaginary time; $0 < \tau < \beta = 1/(k_B T)$]. The saddle point of the resulting action in the static limit gives rise to the conventional mean field approximation in which the second term in Eq.(2) is written as

$$- \tilde{J}_{ij} (\langle b_{ij}^\dagger \rangle b_{ij} + b_{ij}^\dagger \langle b_{ij} \rangle - \langle b_{ij}^\dagger \rangle \langle b_{ij} \rangle) \quad (3)$$

and the average $\psi_m = \psi_{ij} \propto \tilde{J}_{ij} \langle b_{ij} \rangle$ is determined self-consistently (mean field theory).

The effective Hamiltonian we use (see Section III) is of the form of Eq.(2) with the second term in it replaced by Eq.(3). This describes two coupled fluids, namely a fermionic fluid and a bosonic fluid, represented respectively by the on-site electron field $a_{i\sigma}^\dagger$ and the bond Cooper pair field $\psi_{ij} = \psi_m$. The properties of ψ_m needed in our calculation are its mean value $\langle \psi_m \rangle$ (nonzero below T_c) and the fluctuation part of the correlation function $\langle \psi_m \psi_n^* \rangle$ (whose *universal* form for large $|\mathbf{R}_m - \mathbf{R}_n|$ near T_c is what we use). These arise from inter-site interactions of the Cooper pairs ψ_m ; our results are independent of the details of these interactions. A nearest neighbor interaction of the form $C \sum_{\langle mn \rangle} (\psi_m^* \psi_n + \psi_m \psi_n^*)$, with $C > 0$, has been mentioned earlier as a natural possibility [12]. It may arise [12] with $C \propto x$ in a strong correlation picture due to diagonal hole hopping t' .

For a translationally invariant system described by Eq.(2), the electron Green's function satisfies the Dyson equation [26, 27]

$$G^{-1}(\mathbf{k}, i\omega_n) = (G^0)^{-1}(\mathbf{k}, i\omega_n) - \Sigma(\mathbf{k}, i\omega_n), \quad (4)$$

where $\Sigma(\mathbf{k}, i\omega_n)$ ($\omega_n = (2n + 1)\pi/\beta$ is the fermionic Matsubara frequency with n as an integer) is the irreducible self energy, originating from the coupling between bond pairs and electrons with bare propagator $G^0(\mathbf{k}, i\omega_n) = (i\omega_n - \xi_{\mathbf{k}})^{-1}$ where $\xi_{\mathbf{k}} = \epsilon_{\mathbf{k}} - \mu$ and $\epsilon_{\mathbf{k}}$ is the Fourier transform of the hopping $t_{ij} = t_{i-j}$ (μ is the chemical potential).

We use a well-known bosonic fluctuation exchange approximation for $\Sigma(\mathbf{k}, i\omega_n)$ which captures the leading effect of this coupling beyond the 'Hartree' approximation and is shown diagrammatically in Fig.1b. This diagram

describes the exchange of a Cooper pair fluctuation by an electron. In common with general practice, we find Σ (and thence G) by inserting G^0 instead of G in the expression for it [see Eq.(5) below]. This is known to be generally quite accurate [26], e.g. for the coupled electron-phonon system.

Close to T_c , the temporal decay of long-wavelength fluctuations is specially slow (dynamical critical slowing down [36]) so that they can be regarded as quasistatic [12] (i.e. the characteristic frequency scale $\omega_0 \ll k_B T$). Though the decay is 'slow', we assume, as is generally done, that the system is homogeneous. There are *annealing* processes which make it so on the experimental time scale. (There may be intrinsic as well as extrinsic sources of static quenched disorder, e.g., due to the very process of doping itself [37]). Even their effect can be included by approximate configuration averaging. Our approach is similar to that for static critical phenomena where also a homogeneous system is used and all the fluctuations are thermal. The self energy Σ can then be expressed as

$$\begin{aligned} \Sigma(\mathbf{k}, i\omega_n) = & \\ & - \frac{1}{N} \sum_{\mathbf{q}, \mu, \nu} G^0(-\mathbf{k} + 2\mathbf{q}, -i\omega_n) D_{\mu\nu}(2\mathbf{q}) f_\mu(\mathbf{k}, \mathbf{q}) f_\nu(\mathbf{k}, \mathbf{q}) \end{aligned} \quad (5)$$

where N is the total number of Cu sites on a single CuO_2 plane and μ, ν refer to the direction of the bond i.e. x or y . $D_{\mu\nu}(2\mathbf{q}) = \sum_{\mathbf{R}} D_{\mu\nu}(\mathbf{R}) \exp(-i2\mathbf{q} \cdot \mathbf{R})$ is the static pair propagator of Cooper pair fluctuations with $D_{\mu\nu}(\mathbf{R}_{i\mu} - \mathbf{R}_{j\nu}) = \langle \psi_{i\mu} \psi_{j\nu}^* \rangle$. The quantity $f_\mu(\mathbf{k}, \mathbf{q}) = \cos[(k_\mu - q_\mu)a]$ is a form factor arising from the coupling between a tight-binding lattice electron and a nearest-neighbour bond pair. Because of the d -wave LRO described as 'Ne'el' order [12] of the 'planar spin' ψ_m in the bipartite bond-centre lattice, the standard sublattice transformation (i.e. $\psi_m \rightarrow \tilde{\psi}_m = \Delta_m \exp(i\tilde{\theta}_m)$ where $\tilde{\theta}_m = \theta_m$ for x -bonds and $\tilde{\theta}_m = \theta_m + \pi$ for y -bonds) implies $D_{xx}(\mathbf{R}) = D_{yy}(\mathbf{R}) = -D_{xy}(\mathbf{R}) = -D_{yx}(\mathbf{R}) \equiv D(\mathbf{R})$ where $D(\mathbf{R})$ can be written as

$$D(\mathbf{R}_m - \mathbf{R}_n) = \langle \tilde{\psi}_m \rangle \langle \tilde{\psi}_n^* \rangle + \tilde{D}(\mathbf{R}_m - \mathbf{R}_n). \quad (6)$$

Here $\tilde{D}(\mathbf{R})$ is the fluctuation term. The LRO part $\langle \tilde{\psi}_m \rangle \equiv \Delta_d$ leads to a d -wave Gor'kov like gap with $\Delta_{\mathbf{k}} = (\Delta_d/2)(\cos k_x a - \cos k_y a)$; the corresponding electron self energy is $\Sigma(\mathbf{k}, i\omega_n) = \Delta_{\mathbf{k}}^2 / (i\omega_n + \xi_{\mathbf{k}})$. In widely used phenomenological analyses [23] of ARPES data, this form is used above T_c with lifetime effects, both diagonal and off-diagonal in particle number space, added to Σ , i.e.

$$\Sigma(\mathbf{k}, \omega) = -i\Gamma_1 + \frac{\Delta_{\mathbf{k}}^2}{\omega + \xi_{\mathbf{k}} + i\Gamma_0} \quad (7)$$

Here Γ_1 is single-particle scattering rate and Γ_0 is assumed to originate due to finite life-time of *performed* d -wave pairs [23].

We propose here that as described above, the electrons move (above T_c) *not* in a pair field with d -wave LRO which decays in time at a rate put in by hand, but in a nearly static pair field with growing correlation length ξ . We assume, as appears quite natural for a system with characteristic length scale ξ that $\tilde{D}(\mathbf{R}) \sim \exp(-R/\xi)$ for large R , while ξ diverges at T_c . This natural form for $\tilde{D}(R)$ is found, for example, in the Berezinskii-Kosterlitz-Thouless (BKT) theory [36, 38–40] for two dimensions and in a Ginzburg-Landau (GL) theory for all dimensions. As described in Appendix E, it so happens that for large correlation lengths, $\Sigma(\mathbf{k}, i\omega_n)$ is nearly the same as that for preformed d -wave symmetry pairs. Below T_c , $\tilde{D}(R)$ decays as a power law (i.e. $\tilde{D}(R) \sim R^{-\eta}$ with $\eta > 0$) due to order parameter phase or ‘spin wave’-like fluctuations (see the discussion in Section III). We find here the consequences of these for the spectral function, i.e.

$$A(\mathbf{k}, \omega) \equiv -\frac{2}{\pi} \text{Im} [G(\mathbf{k}, i\omega_n \rightarrow \omega + i\delta)], \quad (8)$$

measured in ARPES [4]. $G(\mathbf{k}, i\omega_n)$ is obtained from Eq.(4) with the self energy calculated from Eq.(5) using the aforementioned forms of the pair propagator $\tilde{D}(\mathbf{R})$ [or $D(\mathbf{R})$] for temperatures above and below T_c .

III. ELECTRON SELF ENERGY AND PHENOMENOLOGICAL INPUTS

The tight binding lattice Hamiltonian \mathcal{H} is given by Eq.(2). Near T_c the time dependence of ψ_{ij} can be neglected (except when T_c itself is close to zero where time dependence of ψ_{ij} has significant effects) so that this becomes

$$\mathcal{H} = -\sum_{ij,\sigma} \tilde{t}_{ij} a_{i\sigma}^\dagger a_{j\sigma} - \sum_{\langle ij \rangle} (\psi_{ij} b_{ij}^\dagger + \text{h.c.}). \quad (9)$$

Eq.(9) describes electrons moving in a static but (in general) spatially fluctuating pair potential ψ_{ij} whose correlation length (in our case) diverges as $T \rightarrow T_c$. The effect of the long distance fluctuations on the electrons is captured by the self energy shown in Fig.1b and algebraically described by Eq.(5), with the significant fluctuation wave vector $q \sim \xi^{-1} \ll a^{-1}$. In a regime where the fluctuations in the real pair magnitude Δ_m are short ranged,

$$D(\mathbf{R}) \simeq \langle \Delta(\mathbf{R}) \rangle \langle \Delta(\mathbf{0}) \rangle \langle e^{i[\tilde{\theta}(\mathbf{R}) - \tilde{\theta}(\mathbf{0})]} \rangle \equiv \bar{\Delta}^2 \bar{D}(R) \quad (10)$$

for large R ($R \gg a$) (as evident from Eq.(6), $\tilde{D}(R) \simeq \bar{\Delta}^2 (\bar{D}(R) - | \langle e^{i\tilde{\theta}(\mathbf{0})} \rangle |^2)$). This decoupling between magnitude and long distance phase correlations is accurate for $x \lesssim x_{\text{opt}}$, a manifestation of which is the separation between T^* and T_c . Our calculations based on Eq.(10) are therefore reliable in this doping range. We

use the general form [36] $\bar{D}(R) = (\bar{\Lambda}R)^{-\eta} \exp(-R/\xi)$ (with $\bar{\Lambda} \sim a^{-1}$) in Eq.(5), expanding $\xi_{\mathbf{k}-2\mathbf{q}}$ and $f_\mu(\mathbf{k}, \mathbf{q})$ in powers of \mathbf{q} for $qa \ll 1$. The self energy $\Sigma(\mathbf{k}, i\omega_n)$ (Eq.(5)) is (see Appendix B) then

$$\Sigma(\mathbf{k}, i\omega_n) \simeq \frac{-i \text{sgn}(\omega_n) \Gamma(1-\eta) \bar{\Delta}_{\mathbf{k}}^2}{(\bar{\Lambda}v_{\mathbf{k}})^\eta (v_{\mathbf{k}}/\xi - i \text{sgn}(\omega_n)(i\omega_n + \xi_{\mathbf{k}}))^{1-\eta}}. \quad (11)$$

In this equation, Γ is the well known gamma function and $v_{\mathbf{k}} = \frac{1}{a} \frac{\partial \xi_{\mathbf{k}}}{\partial \mathbf{k}}$ (with $v_{\mathbf{k}} = |v_{\mathbf{k}}|$) is the velocity (expressed in units of energy) obtainable from the energy dispersion $\xi_{\mathbf{k}}$. There is a relatively small particle-hole asymmetric part that adds to $\bar{\Delta}_{\mathbf{k}}^2$ (in the numerator of Eq.(11)) a term proportional to $(i\omega_n + \xi_{\mathbf{k}})$, and is ignored henceforth. The above self energy does not affect the nodal quasiparticles owing to the \mathbf{k} dependence of $\bar{\Delta}_{\mathbf{k}} = (\bar{\Delta}/2)(\cos k_x a - \cos k_y a)$ (of which the second term arises from the form factor appearing in Eq.(5)). Here it is very important to mention that the quantity $\bar{\Delta}_{\mathbf{k}}$ should *not* be confused with the spectral gap $\Delta_{\mathbf{k}}$ that we are going to define below from the position of peak (as a function of ω at a fixed \mathbf{k}) of the spectral function $A(\mathbf{k}, \omega)$. The spectral function $A(\mathbf{k}, \omega)$ (Eq.(8)) is calculated using the self energy of Eq.(11), and the consequent gap ($\Delta_{\mathbf{k}}$) in the electronic spectra is in general different (except at $T = 0$), due to pair fluctuations, from the *input* $\bar{\Delta}_{\mathbf{k}}$ (or $\bar{\Delta}$ that appears in Eq.(10)). An additional term describing the coupling of electrons to short range phase fluctuations (present in our theory, but not discussed here) is probably relevant for nodal quasiparticles. The self energy of Eq.(11) has a nonvanishing imaginary part as $\omega \rightarrow 0$ because of the decay of an electron into one of opposite momentum and small \mathbf{q} Cooper pair fluctuations (see Fig.1 b). Thus the electronic system is a non Fermi liquid.

In order to plot the spectral peaks, e.g. in Fig.2a, we use a small lifetime broadening (~ 3 meV, which is much less than the typical instrumental resolution of ~ 10 meV of ARPES [4, 5]). The nodal peaks, which would be δ -functions in its absence, can then be detected clearly.

Above T_c , we use in Eq.(11) the BKT form

$$\xi(x, T) \simeq a \exp[b'(x)/\sqrt{T/T_c(x) - 1}] \quad (12)$$

and $\eta = \eta_c \equiv T_c/(2\pi\rho_s(T_c)) = 0.25$, corresponding to the universal Nelson-Kosterlitz jump value[36], the BKT transition temperature (say T_{BKT}) has been taken to be actual observed [41] T_c for the cuprates which have small interlayer coupling. The observed T_c can be substantially higher ($\sim 5 - 10$ K) than the underlying BKT transition temperature. This temperature T_{BKT} , though a *fictitious* transition temperature that can only be observed by *switching off* interlayer coupling between CuO_2 planes, is expected to control the correlation length above T_c , away from a narrow 3D-XY critical region [42]. The use of experimentally measured T_c in Eq.(12) as well as the precise value of the exponent $b'(x)$ are not crucial for

the present calculations, although certain details, e.g. the T -dependence of the Fermi arc length close to T_c (within ~ 10 K), can be sensitive to these. For the 2D-XY model [43] $b' \simeq 1.6$. No systematic estimate of either $\xi(x, T)$ or $b'(x)$ exists for the cuprate superconductors. Hence we work with $b'(x)$ obtained using the phenomenological functional of Ref.[12] (see Appendix D for details). The Kosterlitz RG equations [39] predict the asymptotic BKT form for $\xi(T)$ to be valid only over a narrow critical regime above T_c . However, in practice, the BKT form is found [43] to fit the Monte Carlo data for $\xi(T)$ for a 2D-XY model very well over a rather large region of temperature above T_c , till $(\xi/a) \simeq 2$. In the same spirit we use the formula of Eq.(12) over a wide range.

Below T_c , we have used the self energy of Eq.(11) which has been evaluated using the long-distance power-law form $\bar{D}(R) \sim R^{-\eta}$ appropriate for a quasi-LRO state in 2D with $\eta = (T/2\pi\rho_s)$, as well as using a $\bar{D}(R)$ in which a small interlayer coupling is incorporated through a simple anisotropic 3D ‘spin wave’ approximation (see Appendix C). Both approximations produce similar results for $A(\mathbf{k}, \omega)$. The quantity $\eta(x, T) = T/(2\pi\rho_s(x, T))$, with $\rho_s(x, T)$ being the superfluid density, is an input to both of these and we use $\rho_s(x, T)$ estimated from penetration depth data[44] for Bi2212. In addition, the anisotropic 3D form for $\bar{D}(R)$ contains *explicitly* the interlayer coupling characterized by the c -axis superfluid density ρ_s^c or the anisotropy ratio $\varepsilon = (\rho_s^c/\rho_s)^{1/2}$ ($\sim 10^{-2}$ for Bi2212[45]). Close to but below T_c , the experimental values for η exceed (see Fig.5 a) by a large amount the upper limit of η for a pure 2D system i.e. $\eta_c = 0.25$. This fact demonstrates the essential role played by the interlayer coupling in these systems (the observed LRO below T_c is because of it!). Also, the 2D-BKT results that we use above T_c , are not reliable, due to the importance of 3D fluctuations for a narrow temperature regime close to T_c such that $\xi(T) > \varepsilon^{-1}c$ (c is the interlayer spacing); we compare our results with ARPES data outside this range, i.e. outside the critical regime.

Here, it should be mentioned that we have neglected Coulomb interaction between Cooper pairs, which are charged objects, and associated quantum phase fluctuation effects, which can be specially prominent near hole densities (extreme overdoped and underdoped) where T_c vanishes. The power law form used below T_c in our calculation arises due to *longitudinal* phase fluctuations and Coulomb interaction can push these up to plasma frequency, which is quite large (~ 1 eV for cuprates [46, 47]). In this case, the longitudinal phase fluctuations behave classically and are relevant only above a quantum to classical crossover scale T_{cl} . In the absence of dissipation T_{cl} has been estimated to be around 100 K, although dissipation can reduce T_{cl} to a much lower value, ~ 20 K, as has been inferred in Ref.[47]. In our calculation, below T_c , the effects (e.g. the deviation of the \mathbf{k} -space gap structure from d -wave form) of classical phase fluctuations in electron spectral function are considerable only for much higher temperatures, typically close to T_c where $T > T_{cl}$.

Hence we expect the calculated effects to be genuine and natural consequences for phase fluctuating superconductors such as cuprates, and not to be changed much by quantum fluctuation effects except near the end points of $T_c(x)$ curve.

The other phenomenological input, namely $\bar{\Delta}(x, T)$, has been estimated from ARPES data[18, 48, 49] in the following way. (More details are given in Appendix E). Above T_c , the self energy of Eq.(11) can be written a simplified form for $\eta = 0$ (in the actual calculation, above T_c we use $\eta = \eta_c = 0.25$, the BKT jump value), i.e.

$$\Sigma(\mathbf{k}, \omega) = \frac{\bar{\Delta}_{\mathbf{k}}^2}{\omega + \xi_{\mathbf{k}} + i(v_{\mathbf{k}}/\xi)} \quad (13)$$

The resulting peak positions of the spectral function $A(\mathbf{k}, \omega)$ on the Fermi surface (i.e. $\xi_{\mathbf{k}} = 0$) are at $\Delta_{\mathbf{k}}$ which can be easily obtained as

$$\Delta_{\mathbf{k}} = 0 \quad \text{for } |\bar{\Delta}_{\mathbf{k}}| \leq \frac{v_{\mathbf{k}}}{\sqrt{2}\xi} \quad (14a)$$

$$\Delta_{\mathbf{k}}^2 = \bar{\Delta}_{\mathbf{k}}^2 - \left(\frac{v_{\mathbf{k}}}{\sqrt{2}\xi}\right)^2 \quad \text{otherwise} \quad (14b)$$

The above expressions imply that, above T_c , there is a *gapless* (i.e. spectral peak at zero energy) portion corresponding to the \mathbf{k} values such that

$$|\bar{\Delta}_{\mathbf{k}}(T)| \leq \frac{v_{\mathbf{k}}}{\sqrt{2}\xi(T)} \quad (15)$$

As evident from this relation, the extent of this gapless portion along the Fermi surface is temperature dependent since both $\Delta_{\mathbf{k}}$ and ξ depend on temperature. This is the phenomena of ‘Fermi arc’ [17]; we discuss it in more detail in the next section (Section IV). This criterion (Eq.(15)) enables us to deduce a temperature, T_{an} , at which the antinodal gap, $\Delta_{an} = \sqrt{\bar{\Delta}_{an}^2 - (v_{an}/(\sqrt{2}\xi))^2}$, gets completely filled in, i.e. $\Delta_{an}(T_{an}) = 0$ so that the tip of the Fermi arc reaches the antinodal Fermi momentum \mathbf{k}_{an} (here $\bar{\Delta}_{an} \equiv \bar{\Delta}_{\mathbf{k}_{an}}$ and $v_{an} \equiv v_{\mathbf{k}_{an}}$). This implies a self-consistent condition for T_{an}

$$\bar{\Delta}(x, T_{an}) \simeq |\bar{\Delta}_{an}(x, T_{an})| = \frac{v_{an}(x)}{\sqrt{2}\xi(x, T_{an})} \quad (16)$$

With the aid of the above, we estimate the phenomenological input $\bar{\Delta}(x, T)$ at the ARPES-measured pseudogap temperature T^* [48, 49] by identifying it with T_{an} , i.e. $\bar{\Delta}(T^*) \simeq v_{an}/(\sqrt{2}\xi(T^*))$ (the right hand side of this relation is already known as we have estimated ξ from Eq.(12) and $v_{\mathbf{k}}$ is obtained from the band-structure $\xi_{\mathbf{k}}$). Also at $T = 0$, $\bar{\Delta}(0)$ can be deduced from the zero temperature antinodal gap $\Delta_{an}(0)$ measured in ARPES [49], as there $\Delta_{an}(0) = (\bar{\Delta}(0)/2)(\cos(k_{an,x}a) - \cos(k_{an,y}))$. We use a simple interpolation formula, $\bar{\Delta}(x, T) = \bar{\Delta}(x, 0)[1 - \sinh(\alpha(x)T)]$ and utilize the knowledge of $\bar{\Delta}(T)$ at these two temperatures, namely at $T = 0$ and at $T = T^*$, to determine the parameter $\alpha(x)$ (see Appendix E).

This chosen form for $\bar{\Delta}(x, T)$ implies that $\Delta_{\text{an}}(T)$, for a particular $x < x_{\text{opt}}$, varies substantially with T only near $T = T^* \simeq T_{\text{an}}$. This choice qualitatively mimics the experimentally observed temperature-dependence [17, 22, 48] of the antinodal gap (see Appendix E).

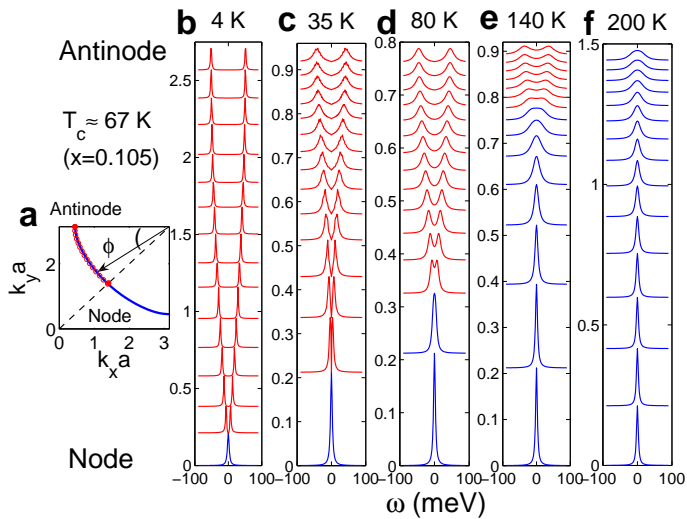


FIG. 2: **The Fermi surface and the spectral density along it.** **a**, Fermi surface (FS) in the first quadrant of the Brillouin zone for $x \simeq 0.11$, a typical value. The angular position ϕ on the Fermi surface is shown. The antinode corresponds to $\phi = 0^\circ$ and node to $\phi = 45^\circ$. **b-f**, Single-particle spectral density $A(\mathbf{k}, \omega)$ at 15 equally spaced points (red circles) on the Fermi surface in **a** shown vertically shifted from node (bottom) to antinode (top), as a function of temperature at $x \simeq 0.11$. Blue and red lines correspond to Fermi arc and gapped portions of FS, respectively.

IV. RESULTS

The results for spectral density are described below and are compared with ARPES experiments for $\omega \lesssim 100$ meV in $\text{Bi}_2\text{Sr}_2\text{CaCu}_2\text{O}_{8+\delta}$ (Bi2212) (with maximum T_c , $T_c^{\text{max}} \simeq 92$ K occurring at $x_{\text{opt}} \simeq 0.16$) across the underlying Fermi surface (FS) (see Appendix A). As mentioned in the preceding section, pairing fluctuation related quantities such as $\eta(x, T)$ [$\eta = (T/(2\pi\rho_s))$] below T_c where $\rho_s(x, T)$ is the measured superfluid density], $\xi(x, T)$ as well as the average local gap [12] $\bar{\Delta}(x, T) = \langle \Delta_m \rangle$ act as inputs to our calculation. The GL-like theory of Ref.[12] provides a unified approach in which all the above quantities and many other results emerge from a single assumed free energy functional; this also leads to results [12] similar to those described below. As remarked earlier, our results are not reliable for extreme underdoped and overdoped regions where $T_c \rightarrow 0$ and consequently quantum phase fluctuation effects can be crucial [12, 35].

Our results for the (particle-hole symmetrized) single

electron spectral density $A(\mathbf{k}, \omega)$ are shown in Fig.2**b-f**. From the spectral density curves (Fig.2**b-f**) for an underdoped system ($x \simeq 0.11$ and $T_c \simeq 67$ K) it is clear that above T_c , for some region of the Fermi surface centered around the nodal point ($\phi = 0$ or $k_x = k_y$), $A(\mathbf{k}, \omega)$ peaks at $\omega = 0$. The extent in \mathbf{k} space over the Fermi surface of this (ungapped quasiparticle excitation) part, normally identified with the ‘Fermi arc’[17], depends on temperature. For any \mathbf{k} outside this region, the spectral function has a peak at a nonzero energy; the value of the peak position is identified conventionally with the energy gap $\Delta_{\mathbf{k}}$. *The Fermi arc emerges above T_c due to the existence of a finite correlation length in the system*, as explained below.

As discussed in the preceding section (Section III), the self energy expression (Eq.(11)) obtained by us implies that the gapped portion terminates (and the Fermi arc begins) when $|\bar{\Delta}_{\mathbf{k}}| \leq v_{\mathbf{k}}/\xi$. One can understand this relation from the fact that a quasiparticle with momentum \mathbf{k} near the Fermi energy moving with a velocity $v_{\mathbf{k}}$ in a spatially fluctuating superconductor having correlated patches of length ξ undergoes scattering over a time interval $\tau \gtrsim \xi/v_{\mathbf{k}}$. The energy of such a quasiparticle is $\sim \bar{\Delta}_{\mathbf{k}}$ so that from the uncertainty relation $\tau \bar{\Delta}_{\mathbf{k}} \gtrsim 1$ or $(\xi/v_{\mathbf{k}})\bar{\Delta}_{\mathbf{k}} \gtrsim 1$. Above T_c , even in the region of the Fermi surface where $\Delta_{\mathbf{k}} \neq 0$, there is (both in our calculations and in experiments) substantial spectral density at zero excitation energy. The simultaneous presence of a nonzero $\Delta_{\mathbf{k}}$ and finite spectral density at zero frequency is the operational definition of pseudogap. Below T_c , the calculated spectral density has two symmetrical peaks at nonzero $\Delta_{\mathbf{k}}$ for all \mathbf{k} except at the node, where the peak is at zero energy.

Fig.3**a** gives an overall pictorial view of the development of the Fermi arc as a function of x and T above T_c . In Fig.3**b**, we plot the arc length versus the reduced temperature, namely (T/T_{an}) , where T_{an} is the temperature at which antinodal pseudogap fills up. The nearly straight line obtained by us over a large range of doping ($0.07 \leq x \leq 0.15$) is seen to compare well with ARPES data over the same range [18]. Qualitatively, since the \mathbf{k} points on the Fermi arc satisfy the condition $|\bar{\Delta}_{\mathbf{k}}| \lesssim v_{\mathbf{k}}/\xi$, this condition is met for a larger \mathbf{k} as $\xi(T)$ decreases on increasing T . Thus the arc length increases with increasing T , and at $T_{\text{an}}(x) \sim T^*(x)$ it is as large as the entire Fermi surface. Conversely, it shrinks to zero at T_c and below because $\xi \rightarrow \infty$ there.

Fig.3**c** shows $T_{\text{an}}(x)$ together with $T_c(x)$ [41] and experimental data for $T^*(x)$ [49] for Bi2212. As mentioned above, T_{an} is taken to coincide with the temperature at which the Fermi arc takes up the full FS, i.e. $|\bar{\Delta}_{\text{an}}(x, T_{\text{an}})| = v_{\text{an}}/(\sqrt{2}\xi(x, T_{\text{an}}))$. Hence $T_{\text{an}}(x)$ is decided by $\bar{\Delta}(x, T) \sim |\bar{\Delta}_{\text{an}}(x, T)|$ and $\xi(x, T)$, both of which are phenomenological inputs to our calculations (v_{an} and \mathbf{k}_{an} are obtained from the energy dispersion $\xi_{\mathbf{k}}$). For $\xi(x, T)$ we use the BKT form of Eq.(12). We have already discussed the choice of the exponent $b'(x)$ appearing in Eq.(12) in Section III and we take a to be

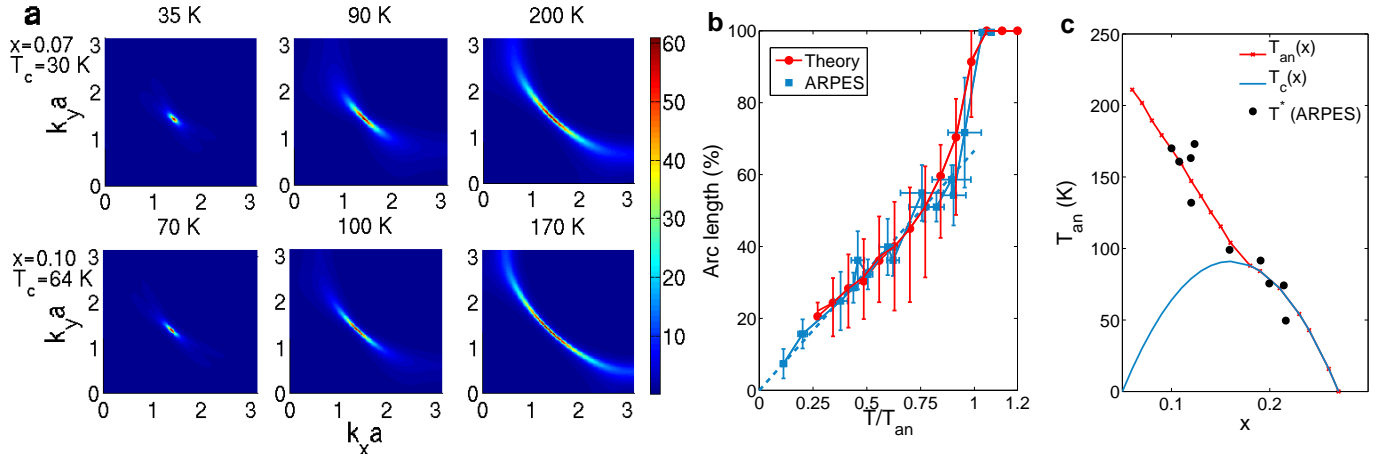


FIG. 3: **Spectral properties above T_c .** **a**, Colourmap of $A(\mathbf{k}, \omega = 0)$ over the first quadrant of the Brillouin zone for two values of x at different temperatures. The Fermi arc is easily picked out visually. The colourbar indicates the value of $A(\mathbf{k}, \omega = 0)$ (in units of $3 \times 10^{-3} \text{ meV}^{-1}$). **b**, The arc length vs. T/T_{an} curve excluding the temperature region within ~ 15 K of T_c (see Appendix D), averaged over the entire doping range ($x \lesssim x_{opt}$). On the y -axis, 0% is the node and 100% is the antinode. The experimental data are from Ref.[18]. The vertical error bars in the theoretical points indicate the variation of the arc length at different x for a given $T/T_{an}(x)$. **c**, The antinodal pseudogap filling temperature T_{an} as a function of x is compared with the data for the pseudogap temperature T^* from ARPES [48, 49]. The parabolic $T_c(x)$ curve [41] used in our calculation is also shown.

the square planar Cu lattice constant, thus completely fixing $\xi(x, T)$ for a given x and T . The main features of our results are not crucially dependent either on the specific form of $\xi(x, T)$ used here or on the particular chosen value of $b'(x)$ (see Appendix D). The other input $\bar{\Delta}(x, T)$ (Appendix E) is fixed by enforcing T_{an} , obtained via the relation $\bar{\Delta}(x, T_{an}) \simeq v_{an}/(\sqrt{2}\xi(x, T_{an}))$, to be close to the ARPES data[49] for the antinodal pseudogap filling temperature $T^*(x)$ i.e. the pseudogap temperature scale measured in ARPES. Thus $T_{an}(x)$ is *preordained* to be nearly same as $T^*(x)$ in our calculation, Fig.3c manifests this fact.

Some other spectral features observed as T decreases through T_c are shown in Fig.4. Each of the left figure panels (Fig.4a, c) exhibits a particular spectral property (see below) over the entire FS (see Fig.2a), for a typical $x \simeq 0.11$ at several temperatures. In the respective right panels (Fig.4b, d) we show the same spectral quantities specifically at the antinode ($\phi = 0$) as a function of temperature for various x . The pseudogap is widely characterized [18, 48] by the function $L(\phi) = 1 - A(\phi, 0)/A(\phi, \Delta)$ that quantifies the loss of spectral weight $A(\phi, \omega)$ for energy $\omega = \pm\Delta(\phi)$ at angular position ϕ (Fig.2a) on the FS. If there is a nonzero gap in the excitation spectrum, and there are no zero energy excitations (as in a BCS superconductor at $T = 0$) $L(\phi) = 1$; if there is no gap (real or pseudo) $L(\phi) = 0$. Intermediate values (i.e. $0 < L(\phi) < 1$) imply a pseudogap. The evolution of $L(\phi)$ as T decreases through T_c describes how the pseudogap develops into a real gap. This is shown in Fig.4a. It agrees qualitatively with that obtained from ARPES [48]. Experiments show a

nonzero $A(\mathbf{k}, \omega = 0)$ (or $L(\phi) < 1$) below T_c as well, unlike in our theory where below T_c , $L(\phi) = 1$, except at $\phi = 45^\circ$ where it is zero. The difference is presumably due to neglect of some causes of intrinsic spectral line-shape broadening, not included in our model, and finite instrumental resolution of ARPES. Above T_c as well, the calculated $L(\phi)$ in the pseudogapped portion is less (by about 20%) than the experimental values, probably due to such effects. In Fig.4a, we have (arbitrarily) multiplied our results by a related factor (~ 1.2) for comparison with experiment. The spectral loss at the antinodal point i.e. $L(\phi = 0) \equiv L_{an}$ is exhibited in Fig.4b for several values of x as a function of T . L_{an} decreases almost linearly with temperature in line with observations[48] and vanishes at $T = T_{an}$.

Another aspect of the spectral function $A(\mathbf{k}, \omega)$ is shown in Fig.4c, in which the full width at half maximum (FWHM) of the peak is plotted as a function of ϕ , again for $x \simeq 0.11$. We notice a maximum in it which coincides with the ϕ location of the Fermi arc tip. Similar features can be deduced from the ARPES spectra[48]. We also find in Fig.4d that while the FWHM of the antinodal peak increases substantially with T below T_c in the underdoped case, it does not change much for the overdoped cuprate, slightly beyond optimal doping. This is what is observed[19]. Again, the experimental widths are seen to be around 20 meV larger than the calculated ones, perhaps due to the same neglect of some intrinsic and extrinsic quasiparticle lifetime effects mentioned earlier.

Possibly the most widely explored property of a superconductor is the energy gap $\Delta_{\mathbf{k}}$ or $\Delta(\phi)$. The apparent deviation ('bending') of the gap below T_c , inferred from

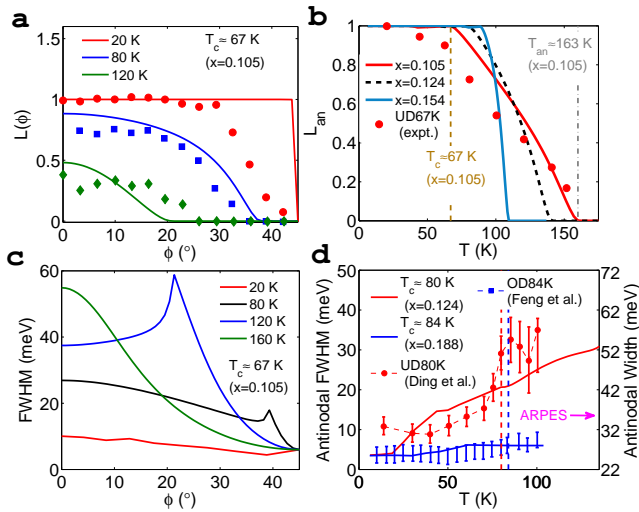


FIG. 4: **Spectral properties both above and below T_c .** **a**, Loss of low energy spectral weight $L(\phi)$ (see text for definition) for three temperatures at $x \simeq 0.11$. The symbols correspond to the experimental data [48] at same temperatures for an underdoped (UD) sample with $T_c = 67$ K, $T^* \simeq 150$ K. **b**, Filling of the antinodal pseudogap (quantified by L_{an}) with temperature for three values of x . **c**, Width (FWHM) of the spectral peaks along the FS for $x \simeq 0.11$. **d**, Variation of the width of the antinodal peak with temperature ($< T_{an}$) for an underdoped ($x \simeq 0.12$) and an overdoped ($x \simeq 0.19$) sample, compared with antinodal widths at the same x values extracted from ARPES data in Refs.[19, 20]. Vertical dashed lines indicate the corresponding T_c 's.

ARPES [21, 22], from the d -wave form has been the subject of a great deal of current interest, leading to speculation that there are two gaps in high- T_c superconductors [50]. We have obtained the gap $\Delta_{\mathbf{k}}$ from the peak position of the calculated spectral function $A(\mathbf{k}, \omega)$ for a fixed \mathbf{k} as mentioned earlier and conclude from the results (see Fig.5a) that the ‘bending’ is due to the coupling of the electron to thermal phase fluctuations (‘spin waves’) below T_c . As expected from such an origin, it is large close to T_c , and small as $T \rightarrow 0$. These results confirm that there is only one gap, but that to ‘uncover’ it, effects of coupling to pair fluctuations (‘spin waves’) have to be included.

Below T_c , because of the LRO in the Cooper pair amplitude, the electrons move in a lattice periodic pair potential while *occasionally* getting scattered from the thermal ‘spin wave’ fluctuations around the ordered state, so that the eigenstates have coherent quasiparticle features. One consequence, shown in Fig.5b, is that the height (A_{an}^p) of the coherent antinodal peak at $\omega = \pm\Delta_{an}$ follows closely the T -dependence of $\eta^{-1} \propto (\rho_s/T)$. A similar empirical correlation has been reported in Refs.[19, 20]. At a given temperature, A_{an}^p is proportional to $\rho_s(x, T)$. This is shown in the inset of Fig.5b for a particular value of T as a function of x .

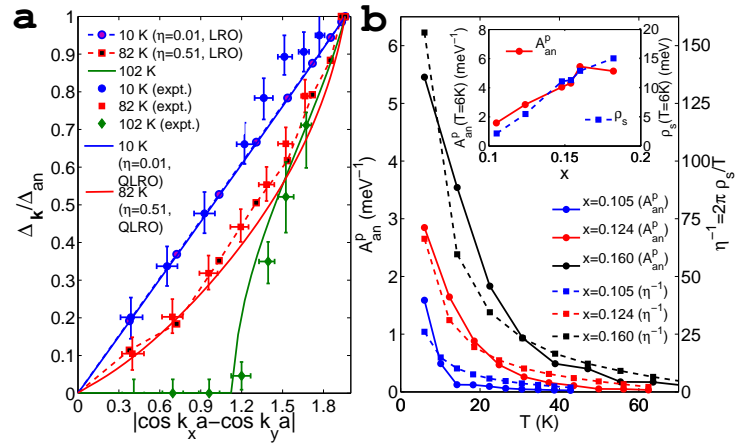


FIG. 5: **Spectral properties below T_c .** **a**, Deviation of $\Delta_{\mathbf{k}}$ from the d -wave form, $|\cos k_x a - \cos k_y a|$, below T_c for $x = 0.16$ is compared with $\Delta_{\mathbf{k}}$ obtained in ARPES[22]. At low temperature ($T = 10$ K), $\Delta_{\mathbf{k}}$ follows the canonical d -wave form (a straight line), but bends away considerably from it close to T_c . For $T < T_c$, we have shown $\Delta_{\mathbf{k}}$ obtained for both the true LRO phase (i.e. $D(R \rightarrow \infty) = |\langle \psi_m \rangle|^2 \neq 0$) and the quasi-LRO or QLRO phase (i.e. $D(R) \sim R^{-\eta} \xrightarrow{R \rightarrow \infty} 0$) (see Methods). The quantity $\eta \propto T/\rho_s$ or the superfluid density $\rho_s(x, T)$ has been estimated from the penetration depth data of Ref.[44]. **b**, The antinodal peak height A_{an}^p vs. T tracks $\rho_s(T)/T$ vs. T . **Inset** At low temperatures ($T = 6$ K) $A_{an}^p(x)$ closely follows $\rho_s(x)$, especially in the underdoped side ($x \lesssim 0.16$).

V. DISCUSSION

Our work is a comprehensive exploration of the consequence of the (inevitable) coupling between electrons and Cooper pair fluctuations constituted of the same electrons in a two dimensional model for the cuprates with a square lattice. Underlying this is a picture of the superconducting transition as a continuous approach to long range order characterized by nonzero phase stiffness so that the pair (phase) correlation length ξ diverges at T_c . (One way this can happen, which is the mechanism discussed in an earlier paper [12] by us in a Ginzburg-Landau-like theory of superconductivity in the cuprates, is the following. Nearest neighbor spin singlet pairs are the basic degree of freedom, and are preformed well above T_c for optimal and suboptimal hole density. Their nearest neighbor phase dependent interaction of ‘AF’ type leads to d -wave symmetry LRO below T_c).

We have obtained here explicitly the self energy $\Sigma(\mathbf{k}, i\omega_n)$ of an electron moving in the field of Cooper pairs whose d -wave symmetry correlation length ξ diverges as $T \rightarrow T_c^+$. This is done very generally, e.g. assuming that the large distance ($R \gg a$) phase correlator function is of the form $R^{-\eta} \exp(-R/\xi)$, where η is the anomalous dimension. In actual calculations we use the specific forms (and values where appropriate) for

η and ξ from the BKT theory [38–40] without making any further assumptions regarding η and ξ . Since the BKT theory predicts somewhat lower T_c compared to experiment ($T_c - T_{\text{BKT}} \sim 5 - 10$ K) and since the effect of small interlayer coupling which leads to the observed three dimensional (XY) critical behavior very close to T_c is neglected, we compare our results for spectral function $A(\mathbf{k}, \omega)$ with ARPES experiments outside a regime $\delta T \simeq 10 - 15$ K from T_c . In this paper, we concentrate on ARPES results because ARPES represents real space averaged measurements. We do not address STM (Scanning Tunnelling Microscopy) results because the latter is a spatially local measurement sensitive to local inhomogeneities.

The lowest order vertex correction to the self energy shown in Fig. 1a vanishes identically above T_c . This is because the vertex correction involving the Cooper pair correlation function $\langle \psi_m \psi_n^* \rangle$ requires the anomalous electron propagator to be non zero. The latter is identically zero since there is no long range superconducting order. The part of the vertex correction involving $\langle \psi_m^* \psi_n^* \rangle$ (or $\langle \psi_m \psi_n \rangle$) is zero because such functions vanish due to ‘isotropy’ or ‘XY-symmetry’ in the space of two-component ‘spin’ $\psi_m = (\Delta_m \cos \theta_m, \Delta_m \sin \theta_m)$. Below T_c , the correction can be calculated exactly as in the classic work of Migdal [51]. The internal phonon propagator of the Migdal calculation is replaced here by the collective phase fluctuation or spin wave or Goldstone mode propagator, so that the correction is $\sim (T_c/\epsilon_F) \sim 10^{-2} \ll 1$. However, higher order vertex corrections are nonzero. These have not been calculated. The internal ‘bosonic’ or pair fluctuation propagator is the true one, not the bare one, since it is described in terms of the observed transition temperature T_c which fully includes dressing or renormalization effects. The approximation made is that the bare fermion (electron/hole) propagator is used in calculating the self energy instead of the dressed one. Experience with the Eliashberg approximation in phonon induced Cooper pair theory (BCS) as well as calculations for coupled electron phonon systems in the normal state show that this is reasonable. We would like to point out that the role of the ‘boson’ here is not to form Cooper pairs (as in the celebrated BCS theory); the spin singlet nearest neighbour Cooper pairs are already formed while the interaction between them leads to the emergence of d wave symmetry superconductivity (long range order or LRO) below T_c as a collective effect. The ‘boson’ of Fig. 1a is the correlation at large distance between d -wave symmetry or collective Cooper pair fluctuations, whose length scale diverges at T_c .

We do *not* attempt to explain the broad part of the one electron Green function [4, 30, 49], specially prominent away from the node, both above and below T_c (this ‘incoherent’ part may well be a strong correlation effect). We assume however that at low excitation energies there is a ‘quasiparticle’ part in the ‘bare’ one electron Green function, with weight $z_{\mathbf{k}}$ (the corresponding Green function, that we calculate here, only gets scaled

by $z_{\mathbf{k}}$, i.e. $G(\mathbf{k}, i\omega_n) \rightarrow z_{\mathbf{k}}G(\mathbf{k}, i\omega_n)$, so that the area under the quasiparticle part of the spectral function $A(\mathbf{k}, \omega)$ is $z_{\mathbf{k}}$ [30]). In strongly correlated system $z_{\mathbf{k}}$ is usually \mathbf{k} -independent [30]. Recent QMC simulations [52, 53] of the one band Hubbard model in two dimensions (widely believed to be appropriate for the cuprates) shows that for strong correlations, there is indeed a quasiparticle part to the one electron Greens function, and that the quasiparticle residue $z_{\mathbf{k}}$ is weakly \mathbf{k} dependent. Presumably, such a z can be absorbed into a definition of renormalized $\tilde{\Delta}^2$, i.e. $(\tilde{\Delta}^2)_{\text{renorm}} = (\tilde{\Delta}^2 z)$ while evaluating $G(\mathbf{k}, \omega)$ using the Dyson equation (Eq.(4)) and the self energy expression of Eq.(5), as $G^0(\mathbf{k}, \omega) \rightarrow zG^0(\mathbf{k}, \omega)$ there. The electronic self energy we calculate as a result of coupling to pair fluctuations depends strongly on \mathbf{k} ; in particular it vanishes at the nodal point.

There have been a large number of calculations of the electron spectral density in cuprates under more specific assumptions and addressing particular experimental findings, e.g. the Fermi arc or the pseudogap. We mention below some that we are aware of. None, as far as we know, compare theoretical results with those of actual experiments explicitly, over this wide a range of temperature, doping, experiments and phenomena or uses this picture of the superconducting phase transition.

Many earlier calculations of the effect of phase fluctuations (e.g. Franz and Millis [24], Berg and Altman [25]) assume that these are connected specifically with supercurrents surrounding thermal vortices. While we use the BKT model, which describes the superconducting transition as due to vortex-antivortex unbinding, and the associated correlation length ξ (Eq.(12)), our form for the self energy (Eq.(11)) is independent of the actual mechanism for the phase fluctuation spectrum or the way ξ diverges approaching T_c , depending only on the generally valid form for the spatial dependence of the correlation function of the phase fluctuations. Some other recent calculations (Micklitz and Norman [55], Senthil and Lee [54]) either use different forms for $D(R)$ or assumes implicitly that $\eta = 0$ and $\xi = \infty$. The latter implies preformed d -wave symmetry pairs which is almost the prevailing belief in the field. In our approach, d -wave symmetry long range order develops at T_c ; above it this begins to *emerge* as a collective phenomenon as $\xi \rightarrow \infty$. A recent calculation by Tsvetlik and Essler [56] is similar in spirit to ours, but in our opinion it is too strongly tied to the anisotropic Kondo limit. Perhaps the closest is the recent numerical calculations by Li and coworkers, who have analyzed the electron self energy Σ via Monte Carlo sampling of 2D-XY model [57] as well as the Hubbard-Stratonovich transformed version [58] of the pair attraction term of Eq.(2) using an involved numerical technique. Their results are similar overall to some of those described here, e.g. in Fig. 3a.

Our approach for calculating the low energy excitation spectrum of electrons coupled to quasi static long-wavelength fluctuations implies that an electron decays into another with *nearly* opposite momentum and a

Cooper pair fluctuations with small momentum $2\mathbf{q}$. This is taken to be the only contribution to quasiparticle decay near the Fermi energy. We do not obtain or emphasize finite Cooper pair life-time effects, generally called ‘dynamic’ effects in the literature, and mostly included empirically to fit ARPES data. We also do not use results from BCS theory which being a mean field theory, can not, we believe, describe accurately the region above T_c (and say, below T^*) since here local Cooper pairs (nearest neighbor spin singlets) exist, but condense collectively into a state of d -wave symmetry LRO only at T_c .

As mentioned earlier, a variety of *exotic* mechanisms, such as stripes [16], d -density wave [13] and time reversal symmetry breaking orbital current state [14], have been suggested and invoked to describe the phenomena observed in the cuprates (especially above T_c). Our work provides an explanation in terms of a simple, inevitable process. We believe that the results, and their agreement with experiments, strongly support our mechanism [12] of nearest neighbor Cooper pairs, and long-range d -wave symmetry order emerging as a collective effect arising from short-range interaction between these pairs. This probably points to the way in which, we believe, high- T_c superconductivity will be understood.

We do not include here the effect of coupling to additional short-range fluctuations which we find to be present. These may have a decisive effect on nodal quasiparticle life-time as well as on linear resistivity in the strange metal phase. We have also not emphasized particle-hole symmetry breaking terms in $A(\mathbf{k}, \omega)$ which we have calculated. Our approach implies that fluctuation effects, very small in conventional superconductors, are sizable in the cuprates and are present over a wide temperature range.

Acknowledgments

We thank S. Mukerjee and U. Chatterjee for useful discussions. S.B. would like to acknowledge CSIR (Govt. of India) and DST (Govt. of India) for support. T.V.R. acknowledges research support from the DST (Govt. of India) through the Ramanna Fellowship as well as NCBS, Bangalore for hospitality. C.D. acknowledges support from DST (Govt. of India).

Appendix A: Determination of the Fermi surface

The chemical potential μ is computed by setting $\int_{-\infty}^{\infty} d\omega \sum_{\mathbf{k}} f(\omega) A(\mathbf{k}, \omega) = (1-x)$ (here $f(\omega) = 1/(e^{\beta\omega} + 1)$ is the Fermi function) and the underlying Fermi surface is defined from the locus of $\xi_{\mathbf{k}} = 0$. We have implemented other FS criteria in our calculation e.g. the locus of the minimum of $\Delta_{\mathbf{k}}$ [18] as well as the locus of the maximum of $A(\mathbf{k}, \omega = 0)$. The main features of the results (Figs.2-5) remain unaltered for different FS criteria.

Appendix B: Evaluation of self energy

When the pair correlator $D(\mathbf{R})$ in Eq.(6) is sufficiently long-ranged (below T_c at all temperatures, and above T_c for temperatures such that $\xi(T) \gg a$), its Fourier transform $D(2\mathbf{q}) = \sum_{\mathbf{R}} D(\mathbf{R}) \exp(-i2\mathbf{q}\cdot\mathbf{R})$ is sharply peaked around $\mathbf{q} = 0$ and one can expand $\xi_{\mathbf{k}-2\mathbf{q}}$ and $f_{\mu}(\mathbf{k}, \mathbf{q})$ in Eq.(5) in powers of \mathbf{q} , so that $\Sigma(\mathbf{k}, i\omega_n)$ can be approximated as,

$$\Sigma(\mathbf{k}, i\omega_n) \simeq \mathcal{R}(\cos k_x a - \cos k_y a)^2 + \dots, \quad (\text{B1})$$

where $\mathcal{R} = N^{-1} \sum_{\mathbf{q}} D(2\mathbf{q}) / (i\omega_n + \xi_{\mathbf{k}} - 2\mathbf{v}_{\mathbf{k}}\cdot\mathbf{q})$. In Eq.(B1), we have not shown explicitly particle-hole non-symmetric contributions to $\Sigma(\mathbf{k}, i\omega_n)$ for which we have obtained closed form expressions. This can be recast using standard mathematical identities into forms suitable for analytical and numerical calculations, i.e.

$$\mathcal{R} = -\frac{i \operatorname{sgn}(\omega_n)}{4} \int_0^{\infty} ds e^{i \operatorname{sgn}(\omega_n)(i\omega_n + \xi_{\mathbf{k}})s} D(sv_{\mathbf{k}}), \quad (\text{B2})$$

The above expression utilizes only the *real-space pair correlator* $D(R)$ (Eq.(6)). This procedure is very different from the way self energy is generally calculated using momentum space form of $D(R)$ (see e.g. Refs.[54, 55]). For instance, using $D(R) \simeq \bar{\Delta}^2(T) \bar{D}(R)$ (Eq.(10)) along with $\bar{D}(R) = (\tilde{\Lambda}R)^{-\eta} \exp(-R/\xi)$ ($\tilde{\Lambda} = e^{-0.116} 2\sqrt{2\pi}/a$ is related to upper wave-vector cutoff [36]) results in the self energy expression of Eq.(11). As evident, the integration variable s in Eq.(B2) has dimension of time or inverse energy and hence the presence of $D(sv_{\mathbf{k}}) \sim \exp(-sv_{\mathbf{k}}/\xi)$ in Eq.(11) cuts off the contributions for large timescales corresponding to $s \gg \xi/v_{\mathbf{k}}$. Below T_c , $D(R)$, calculated from a spin wave approximation incorporating finite interlayer coupling (see below), is used in Eq.(B2) to obtain $\Sigma(\mathbf{k}, i\omega_n)$ by numerical integration. This also demonstrates the usefulness of Eq.(B2) for evaluating self energy using arbitrary form of the real-space pair correlator as it amounts to carrying out a one dimensional integral, either analytically or numerically.

Appendix C: Pair correlator $D(\mathbf{R})$ below T_c in the presence of non-zero interlayer coupling

Below T_c , we estimate the phase correlator $\bar{D}(R) = \langle e^{i(\tilde{\theta}(\mathbf{R}) - \tilde{\theta}(0))} \rangle$ of Eq.(6) using the well known harmonic spin wave approximation i.e. the elastic free energy functional for an anisotropic 3D system,

$$\begin{aligned} \mathcal{F}_{\text{SW}} &= \frac{\rho_s(T)}{2c} \int d\mathbf{r} [(\partial_x \varphi)^2 + (\partial_y \varphi)^2] \\ &+ \frac{\rho_s^c(T)c}{2a^2} \int d\mathbf{r} (\partial_z \varphi)^2, \end{aligned} \quad (\text{C1})$$

where $\partial_x \equiv \frac{\partial}{\partial x}$ and c is the interlayer spacing. As mentioned earlier, $\rho_s = \rho_s^{ab}$ and ρ_s^c are the ab -plane and c -axis

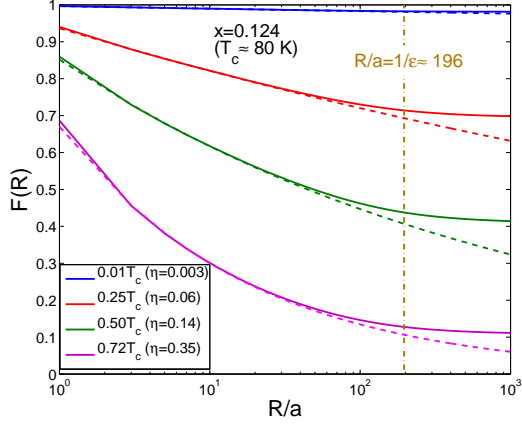


FIG. 6: **Phase correlator $\bar{D}(R)$ below T_c .** $\bar{D}(R)$ (solid lines) estimated using Eq.(C3) for $x = 0.124$ at four different temperatures. Also shown are the corresponding 2D correlator $\bar{D}_{2D}(R)$ (dashed lines). The vertical dashed line indicates the length scale below which $\bar{D}(R) \simeq \bar{D}_{2D}(R)$.

superfluid density, respectively. The phase correlator can be written [36] as $\bar{D}(R) = \exp(-g(R))$, with

$$g(R) = \frac{T_c}{\rho_s(T)} \int_{-\pi/a}^{\pi/a} \frac{dq_x dq_y}{(2\pi)^2} \int_{-\pi/c}^{\pi/c} \frac{dq_z}{2\pi} \frac{1 - e^{i\mathbf{q}\cdot\mathbf{R}}}{q_x^2 + q_y^2 + \varepsilon^2(cq_z/a)^2}, \quad (\text{C2})$$

Here $\varepsilon = (\rho_s^c/\rho_s)^{1/2}$ and $\mathbf{R} = (R_x, R_y, 0)$ is in the xy -plane. Finally one obtains,

$$\bar{D}(R) = \exp \left[- \left(g_{\text{LRO}} - \frac{\eta}{\pi\varepsilon} \int_0^\Lambda dq J_0 \left(\frac{qR}{a} \right) \tan^{-1} \left(\frac{\varepsilon\pi}{q} \right) \right) \right] \quad (\text{C3})$$

Here, J_0 is the ordinary Bessel function, and $g_{\text{LRO}} = \frac{\eta}{2\pi\varepsilon} [\Lambda\pi - 2\Lambda \cot^{-1}(\varepsilon\pi/\Lambda) + \varepsilon\pi \ln(1 + (\Lambda/\pi\varepsilon)^2)]$ with $\Lambda = 2\sqrt{\pi}$ and $\eta = T/(2\pi\rho_s)$. The phase correlator $\bar{D}(R)$ is shown in Fig.6a for $x = 0.124$ at different temperatures. $\bar{D}(R)$ starts from $\bar{D}(0) = 1$ and decreases to a constant value $\bar{D}_{\text{LRO}} = \exp(-g_{\text{LRO}})$ as $R \rightarrow \infty$. The fluctuation part $\tilde{D}(\mathbf{R})$ (Eq.(6)) can be obtained as $\tilde{D}(R) \simeq \bar{\Delta}^2(T)(\bar{D}(R) - \bar{D}_{\text{LRO}})$. In Fig.6a, we also show the corresponding 2D phase correlator ($\bar{D}_{2D}(R) = (\tilde{\Lambda}R)^{-\eta}$) which is appropriate for a QLRO phase as $\bar{D}_{2D}(R \rightarrow \infty) \rightarrow 0$; $\bar{D}_{2D}(R)$ is also obtained from the spin wave approximation for a 2D system[36]. For $a \lesssim R < \varepsilon^{-1}a$, $\bar{D}(R) \simeq \bar{D}_{2D}(R)$ i.e. the system effectively behaves as two dimensional. Both the spin wave approximations, the anisotropic 3D and pure 2D, are expected to be quantitatively correct only at low temperatures. Especially the estimation of the LRO part of $\bar{D}(R)$ i.e. \bar{D}_{LRO} obtained

using the anisotropic 3D calculation is only accurate at very low temperature for large anisotropy or small ε . In our calculation, this fact is manifestly observed e.g. in the variation of the antinodal gap Δ_{an} with temperature for $T < T_c$ (see Fig.8b). The planar superfluid density $\rho_s(T)$ is estimated from the measured ab -plane penetration depth [44] for Bi2212 using $\rho_s = \Phi_0^2 c / (16\pi^3 \lambda_{ab}^2)$; Φ_0 is the fundamental flux quantum and we take $c = 15 \text{ \AA}$ as suitable for Bi2212. For the anisotropy ratio ε (assumed to be temperature independent), we use the empirical formula [45] $\varepsilon(x) = \varepsilon(x_{\text{opt}})(x - x_u)/(x_{\text{opt}} - x_u)$, where $x_{\text{opt}} = 0.16$ is the optimal hole doping and $x_u = 0.047$ is the end point of the $T_c(x)$ dome in the underdoped side, with $\varepsilon(x_{\text{opt}}) \simeq 1/133$.

Appendix D: Correlation length $\xi(x, T)$ above T_c

As mentioned in Section III, $\xi(x, T)$ is estimated using the BKT form [36] i.e. $\xi(x, T) \simeq a \exp(b'(x)/\sqrt{T/T_c(x) - 1})$. To obtain the actual correlation length, one needs the value of the dimensionless quantity $b'(x)$, which is in the exponent. This is a nonuniversal number of order 1. For thin superconducting films its value ranges [42] from 1 to 4. Unfortunately for cuprates no such estimate exists for b' (presumably doping and material dependent). We have estimated b' using a GL-like functional in Ref.12. As shown there, with appropriate choices of a few parameters as input in the GL-like functional, it can be used to explain and reconcile a wide variety of experimental data for the cuprates e.g. those for $T_c(x)$, $\rho_s(x, T)$, and the contribution of pair degrees of freedom to the electronic specific heat. The quantity $b'(x)$ has been estimated there in the following manner. In two dimensions, the system described by the model undergoes a BKT transition at a temperature $T_{\text{BKT}}(x)$. So, the correlation length $\xi(x, T)$ is expected to follow the aforementioned BKT form above $T_c(x)$, where $T_c(x)$ is identified with $T_{\text{BKT}}(x)$. In such a scenario, as predicted by BKT theory [36], the superfluid density below $T_c(x)$ is given by the formula [36, 59] $\rho_s(x, T) = \rho_s(T_c(x))[1 + b(x)\sqrt{1 - T/T_c(x)}]$ near the transition. The BKT theory further predicts a universal relation[59] between b' and b , namely $bb' = \pi/2$. Keeping this fact in mind, we calculate $\rho_s(x, T)$ below T_c from a Monte Carlo simulation of the GL model[12] and fit the results to the above mentioned BKT form for $\rho_s(x, T)$ to estimate $b(x)$ and thence $b'(x)$. The results for $b'(x)$ are shown in the inset of Fig.7a).

We show $\xi(T)$, estimated using $b'(x)$ obtained in this manner, in Fig.7a for four different x values. These results for $\xi(x, T)$ have been used in Eq.(11) to calculate the spectral properties above $T_c(x)$, as reported in Figs.2-5 of the main paper. We have also used the constant value $b'(x) = 1.59$, expected for a 2D-XY model[43], to repeat the same calculations. The results in the two cases only differ in details and their main features over the entire x range are found to be robust with respect to different

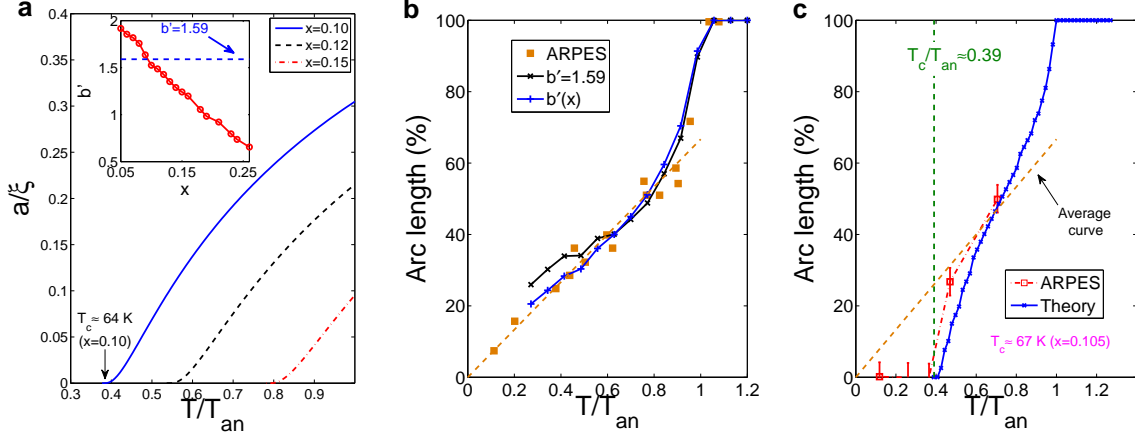


FIG. 7: **Correlation length $\xi(x, T)$ and Fermi arc length.** **a**, The correlation length ξ , which controls the approximate linear temperature dependence of arc length with temperature in Fig.3 **b**, is shown as a function of dimensionless temperature $T/T_{\text{an}}(x)$ for four x values. **Inset:** $b'(x)$ estimated from the GL-like functional of Ref.12. The horizontal dashed line corresponds to $b' = 1.59$, as estimated for a 2D-XY model [43]. **b**, The arc length vs. $T/T_{\text{an}}(x)$ curves (the average curve for the doping range $0.07 \leq x \leq 0.15$) for two different choices of b' , namely $b' = 1.59$ and an x -dependent b' estimated using the functional of Ref.12. The rapid increase of arc length near $T/T_{\text{an}} = 1$ is related with the rapid decrease of $\langle \Delta_m \rangle = \bar{\Delta}(T)$ near T_{an} (see Fig.8). **c**, The arc length as a function of T/T_{an} for $x \simeq 0.11$. ARPES results[18] for the arc length for the same doping at a few values of T/T_{an} are also shown.

choices of $b'(x) \sim 1$ (see Fig.7**b**). These temperature dependence of ξ^{-1} (along with $\langle \Delta_m \rangle = \bar{\Delta}(T)$, see below) governs the behaviour of the arc length as a function of T (see Fig.7**c**). Starting from zero at T_c , the arc length rises steeply with T in a temperature range (~ 15 K) from T_c (the actual value depending on x) to ultimately follow the mean curve shown in Fig.7**b**. In our calculation this temperature range depends primarily on the details of the temperature dependence of ξ close to T_c and hence the range can be tuned by changing b' as well as the T_c appearing in Eq.(12).

We use actual observed T_c values for evaluating ξ from Eq.(12). It is well known that the BKT theory result for T_c (T_{BKT}) in principle can be substantially lower than the observed T_c [42]. Also, we have neglected interlayer coupling which affects $\xi(T)$ and indeed determines the critical behavior very close to T_c (It is 3D-XY [45] and this 3D critical regime is about a degree or two wide). Because of the two reasons, we compare our results for the Fermi arc length in Fig.3 with experiment only beyond a regime $\delta T \sim 10 - 15$ K from T_c . Using our theory, $\xi(x, T)$ itself can be estimated more accurately at a phenomenological level from a detailed comparison with experimental data for the arc length as a function of T , especially in a temperature region close to T_c since $\bar{\Delta}(T)$ is weakly temperature dependent in this regime.

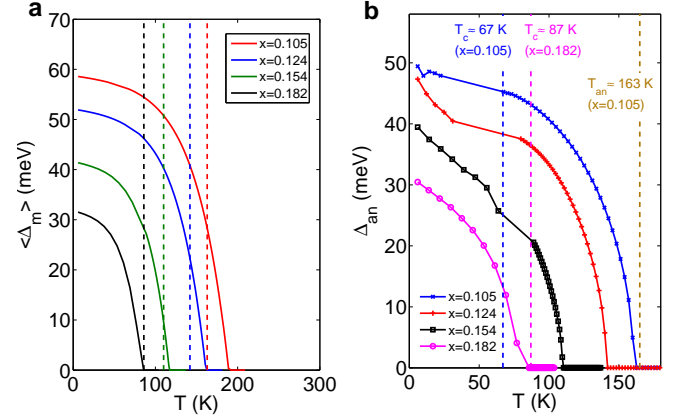


FIG. 8: **Average local gap and antinodal gap.** **a**, $\bar{\Delta}(T) = \langle \Delta_m \rangle$ for four values of hole density. Vertical dashed lines indicate the respective antinodal pseudogap filling temperatures T_{an} . **b**, $\Delta_{\text{an}}(T)$ for the same hole densities.

Appendix E: Fermi arc criterion, average local gap $\bar{\Delta}(x, T)$ and antinodal gap $\Delta_{\text{an}}(x, T)$

As already discussed in Section III, the genesis of the Fermi arc above T_c can be understood from the self energy of Eq.(11). Neglecting the small η in Eq.(11), $\Sigma(\mathbf{k}, \omega) = \Sigma(\mathbf{k}, i\omega_n \rightarrow \omega + i\delta)$ can be written in a simple form depicted in Eq.(13). This is exactly same as the phenomenological form[23, 60] that has been used widely to analyze the ARPES data using a single particle scat-

tering rate Γ_1 and d -wave pairs with finite life-time Γ_0 . In Eq.(13), Γ_0 is replaced by $v_{\mathbf{k}}/\xi$ (the single particle scattering rate is zero for $\eta = 0$), although our picture for its origin is completely different, as described in the main paper.

For \mathbf{k} lying on the Fermi surface ($\xi_{\mathbf{k}} = 0$), the spectral density $A(\mathbf{k}, \omega)$ has a peak at $\omega = 0$ for \mathbf{k} values such that $|\bar{\Delta}_{\mathbf{k}}(T)| \leq v_{\mathbf{k}}/(\sqrt{2}\xi(T))$ and two peaks at $\omega = \pm\sqrt{\bar{\Delta}_{\mathbf{k}}^2(T) - (v_{\mathbf{k}}/(\sqrt{2}\xi(T)))^2}$ otherwise. The former determines the extended region corresponding to the Fermi arc. The antinodal pseudogap $\Delta_{\text{an}} \simeq \sqrt{\bar{\Delta}_{\text{an}}^2 - (v_{\text{an}}/(\sqrt{2}\xi))^2}$ is completely filled in above a temperature T_{an} , at which the end of the arc reaches the antinodal Fermi momentum [61] \mathbf{k}_{an} i.e. the criterion of Eq.(16) is satisfied.

At this point, we would like to reemphasize that both $\bar{\Delta}(x, T)$ and $\xi(x, T)$ are purely phenomenological inputs to our theory. As mentioned in Appendix D, $\xi(x, T)$ has been determined following fairly general considerations related to the superconducting transition at $T_c(x)$ (we use the empirical $T_c(x)$ curve [41] appropriate for Bi2212, see Fig.3c). To choose $\bar{\Delta}(x, T)$, we first demand $T_{\text{an}}(x)$ to be close to the pseudogap filling temperature T^* obtained in ARPES experiments [48, 49]. Since $v_{\text{an}}(x)$

(calculated from the tight-binding energy dispersion $\xi_{\mathbf{k}}$, see Section III) and $\xi(x, T_{\text{an}})$ (Appendix D) are already fixed, Eq.(16) enables us to deduce the value of $\bar{\Delta}(x, T_{\text{an}})$. Also, at $T \simeq 0$, $\bar{\Delta}(x, 0) \simeq \Delta_{\text{an}}(x, 0)$. Using this relation, we obtain the zero temperature antinodal gap $\Delta_{\text{an}}(x, 0)$, again from the ARPES data[49], to estimate the value of $\bar{\Delta}(x, T)$ at $T = 0$. Once both $\bar{\Delta}(x, 0)$ and $\bar{\Delta}(x, T_{\text{an}})$ are known, a simple interpolation formula, $\bar{\Delta}(x, T) = \bar{\Delta}(x, 0)[1 - \sinh(\alpha(x)T)]$, is used to obtain the parameter $\alpha(x)$ so that the function $\bar{\Delta}(x, T)$ is completely determined (Fig.8). This interpolating form is chosen to qualitatively mimic the fact that $\Delta_{\text{an}}(T)$ ($\sim \bar{\Delta}(T)$) varies substantially with temperature only near $T = T_{\text{an}}$, particularly in the underdoped Bi2212, as reported in Ref.48. However, we note that very different temperature variation of $\Delta_{\text{an}}(T)$, i.e. $\Delta_{\text{an}}(T)$ varying considerably with temperature below T_{an} , has been reported in ARPES studies [62, 63] on other cuprates (e.g. Bi2201, La214). These observations suggest that the form of $\bar{\Delta}(x, T)$ may differ substantially from one material to other. Since $\bar{\Delta}(x, T)$ is a phenomenological input to our theory, such issues can not be resolved unless a satisfactory microscopic theory for cuprate superconductivity is developed such that $\bar{\Delta}(x, T)$ is calculable starting from an appropriate microscopic Hamiltonian.

-
- [1] P. A. Lee, N. Nagaosa and X. G. Wen, Rev. Mod. Phys. **78**, 17 (2006).
- [2] *Handbook of High-Temperature Superconductivity: Theory and Experiment*, edited by J. R. Schrieffer and J. S. Brooks (Springer, Berlin, 2007).
- [3] *The Physics of Superconductors*, edited by K. H. Bennemann and J. B. Ketterson (Springer, Berlin, 2003), Vols. I and II.
- [4] A. Damascelli, Z. Hussain, Z. X. Shen, Rev. Mod. Phys. **75**, 473 (2003).
- [5] See the article by J.C. Campuzano, M.R. Norman and M. Randeria in Ref.3.
- [6] T. Timusk and B. Statt, Rep. Prog. Phys. **62**, 61 (1999).
- [7] S. Hüfner et al., Rep. Prog. Phys. **71**, 062501 (2008).
- [8] M. R. Norman, D. Pines and C. Kallin, Adv. Phys. **54**, 715 (2005).
- [9] Y. Wang, L. Li and N. P. Ong, Phys. Rev. B **73**, 024510 (2006).
- [10] L. Li et al., Phys. Rev. B **81**, 054510 (2010).
- [11] V. J. Emery and S. A. Kivelson, Nature **374**, 434-437 (1995).
- [12] S. Banerjee, T. V. Ramakrishnan and C. Dasgupta, Phys. Rev. B **83**, 024510 (2011).
- [13] S. Chakravarty et al., Phy. Rev. B **63**, 094503 (2001).
- [14] C. M. Varma, Phys. Rev. B **73**, 155113 (2006).
- [15] S. A. Kivelson, E. Fradkin and V. J. Emery, Nature **393**, 550 (1998).
- [16] S. A. Kivelson et al., Rev. Mod. Phys. **75**, 1201 (2003).
- [17] Norman, M. R. et al., Nature **392**, 157 (1998).
- [18] A. Kanigel et al., Nature Phys. **2**, 447 (2006).
- [19] H. Ding et al., Phys. Rev. Lett. **87**, 227001 (2001).
- [20] D. L. Feng et al., Science **289**, 277 (2000).
- [21] K. Tanaka et al., Science **314**, 1910 (2006).
- [22] W. S. Lee et al., Nature **450**, 81 (2007).
- [23] M. R. Norman, M. Randeria, H. Ding and J. C. Campuzano, Phys. Rev. B **57**, R11093 (1998).
- [24] M. Franz and A. J. Millis, Phs. Rev. B **58**, 14572 (1998).
- [25] E. Berg and E. Altman, Phys. Rev. Lett. **99**, 247001 (2007).
- [26] G. D. Mahan, *Many-particle Physics* (Springer, India, 2008).
- [27] A. Altland and B. Simons, *Condensed Matter Field Theory* (Cambridge Univ. Press, Cambridge, 2006).
- [28] P. Fazekas, *Lecture Notes on Electron Correlation and Magnetism* (World Scientific, Singapore, 2003).
- [29] P. W. Anderson et al., J. Phys. Condens. Matter **16**, R755 (2004).
- [30] B. Edegger, V. N. Muthukumar and C. Gros, Adv. Phys. **56**, 927 (2007).
- [31] A. Paramekanti, M. Randeria and N. Trivedi, Phys. Rev. B **70**, 054504 (2004).
- [32] P. W. Anderson, G. Baskaran, Z. Zou and T. Hsu, Phys. Rev. Lett. **58**, 2790 (1987).
- [33] G. Baskaran and P. W. Anderson, Phys. Rev. B **37**, 580 (1988).
- [34] M. A. Kastner et al., Rev. Mod. Phys. **70**, 897 (1998).
- [35] Z. Tesanovic, Nature Phys. **4**, 408 (2008).
- [36] P. M. Chaikin and T. C. Lubensky, *Principles of Condensed Matter Physics* (Cambridge Univ. Press, Cambridge, 2004).
- [37] H. Alloul, J. Bobroff, M. Gabay and P. J. Hirschfeld, Rev. Mod. Phys. **81**, 45 (2009).
- [38] V. L. Berezinskii, Sov. Phys.-JETP **32**, 493 (1973).
- [39] J. M. Kosterlitz and D. J. Thouless, J. Phys. C **6**, 1181

- (1973).
- [40] J. M. Kosterlitz, J. Phys. C **7**, 1046 (1974).
- [41] M. R. Persland, J. L. Tallon, R. G. Buckley, R. S. Liu and N. E. Flower, Physica C **176**, 95 (1991).
- [42] G. Blatter, M. V. Feigel'man, V. B. Geshkenbein, A. I. Larkin and V. M. Vinokur, Rev. Mod. Phys. **66**, 1125 (1994).
- [43] P. Olsson, Phys. Rev. B **52**, 4526 (1995).
- [44] W. Anukool, S. Barakat, C. Panagopoulos and J. R. Cooper, Phys. Rev. B **80**, 024516 (2009).
- [45] See the article by T. Schneider in Re.[3].
- [46] A. Paramekanti, M. Randeria, T. V. Ramakrishnan and S. S. Mandal, Phys. Rev. B **62**, 6786 (2000).
- [47] L. Benfatto, S. Caprara, C. Castellani, A. Paramekanti and M. Randeria, Phys. Rev. B **63**, 174513 (2001).
- [48] A. Kanigel et al., Phys. Rev. Lett. **99**, 157001 (2007).
- [49] J. C. Campuzano et al., Phys. Rev. Lett. **83**, 3709 (1999).
- [50] A. J. Millis, Science **314**, 1888 (2006).
- [51] A. B. Migdal, Soviet Physics JETP **1**, 996 (1958).
- [52] B. Moritz et al., New J. Phys. **11**, 093020 (2009).
- [53] A. Macridin, M. Jarrell, T. Maier and D. J. Scalapino, Phys. Rev. Lett. **99**, 237001 (2007).
- [54] T. Senthil and P. A. Lee, Phys. Rev. B **79**, 245116 (2009).
- [55] T. Micklitz and M. R. Norman, Phys. Rev. B **80**, 220513(R) (2009).
- [56] A. M. Tsvelik and F. H. L. Essler, Phys. Rev. Lett. **105**, 027002 (2010).
- [57] Q. Han, T. Li, Z. D. Wang, [arXiv:1005.5497](https://arxiv.org/abs/1005.5497).
- [58] Y-W. Zhong, T. Li and Q. Han, [arXiv:1008.4191](https://arxiv.org/abs/1008.4191).
- [59] V. Ambegaokar, B. I. Halperin, D. R. Nelson, and E. D. Siggia, Phys. Rev. B **21**, 1806 (1980).
- [60] M. R. Norman, A. Kanigel, M. Randeria, U. Chatterjee and J. C. Campuzano, Phys. Rev. B **76**, 174501 (2007).
- [61] \mathbf{k}_{an} is determined from the Fermi surface ($\xi_{\mathbf{k}} = 0$) crossing at the Brillouin zone boundary (see Fig.2a).
- [62] M. Hashimoto et al., Nature Phys. **6**, 414 (2010).
- [63] T. Yoshida et al., Phys. Rev. Lett. **103**, 037004 (2009).